Research article

Low-pressure chromatographic separation and UV/Vis spectrophotometric characterization of the native and desialylated human apo-transferrin

Tomislav Friganović, Antonela Tomašić, Tino Šeba, Ivan Biruš, Robert Kerep, Valentina Borko, Davor Šakić, Mario Gabričević, Tin Weitner [*]

Faculty of Pharmacy and Biochemistry, University of Zagreb, Ante Kovačića 1, 10000 Zagreb, Croatia

A B S T R A C T

Low-pressure pH gradient ion exchange separation provides a fast, simple and cost-effective method for preparative purification of native and desialylated apo-transferrin. The method enables easy monitoring of the extent of the desialylation reaction and also the efficient separation and purification of protein fractions after desialylation. The *N*-glycan analysis shows that the modified desialylation protocol successfully reduces the content of the sialylated fractions relative to the native apo-transferrin. In the optimized protocol, the desialylation capacity is increased by 150 %, compared to the original protocol provided by the manufacturer. The molar absorption coefficients in the near-UV region for the native and desialylated apo-transferrin differ by several percent, suggesting a subtle dependence of the glycoprotein absorbance on the variable sialic acid content. The method can easily be modified for other glycoproteins and is particularly appropriate for quick testing of sialic acid content in the protein glycosylation patterns prior to further verification by mass spectrometry.

1. Introduction

Glycosylation is one of the most common posttranslational modifications of proteins. Nearly all membrane and secreted proteins, as well as numerous intracellular proteins, are modified with complex glycan structures to enable communication, binding, recognition and/or modification of the protein activity. Such modified proteins play a role in almost every biological process and are involved in numerous major diseases [1]. Glycan moieties of glycoproteins are not synthesized using a direct genetic template. Instead, they result from the interplay of several hundred enzymes organized in complex pathways. Increase of interest for glycosylation and other associated processes resulted in the opening of a new field in biology named glycobiology [2, 3]. Changes in the glycosylation pattern can have an important role in cellular recognition and the regulation of gene expression, in addition to the influence on function of proteins. Furthermore, a change of the glycosylation pattern has been associated with numerous pathological conditions [4].

Transferrin is a heavily glycosylated serum protein that binds to and consequently mediates the cellular transport of iron. Reference range of the human serum levels is 1940–3420 mg/L, but this may be increased during pregnancy, therapy with oral contraceptives and/or due to increased synthesis caused by iron deficiency. Lower values are

characteristic for increased catabolism, liver problems, chronic infections, malnutrition, trauma etc. Half-life of transferrin in the serum is about 16 hours. [5]. Transferrin structure consists of 679 amino acids with two glycan structures covalently linked to asparagine residues 413 and 611. Glycan structures can be bi- or tri-antennary and each of them terminates with sialic acid. In normal serum, 85 % is tetra-sialotransferrin and the rest (15 %) is penta- or tri-sialotransferrin [6]. The scheme of human transferrin glycoforms microheterogeneity is shown in Figure 1. Gene mutations can cause defects in glycosylation resulting in inborn errors of metabolism, characterized by deficient or reduced glycosylation and known as congenital disorders of glycosylation (CDGs) [7]. Change of sialylation has also been linked to alcoholism and many pathological states [8, 9]. Nowadays, the analysis of glycosylation change is used as a diagnostic tool for alcoholism and congenital disorders of glycosylation [10, 11]. Importantly, the sialylation of transferrin may alter its fundamental function as iron carrier and may also affect the transfer of iron into liver [12, 13].

Ferroptosis, a newly identified form of non-apoptotic regulated cell death characterized by iron-dependent accumulation of lipid peroxides plays a vital role in the treatment of tumours, renal failure or ischemia reperfusion injury [14]. Both transferrin and transferrin receptor 1 (TFR1) are required for ferroptosis induction [15], and this might
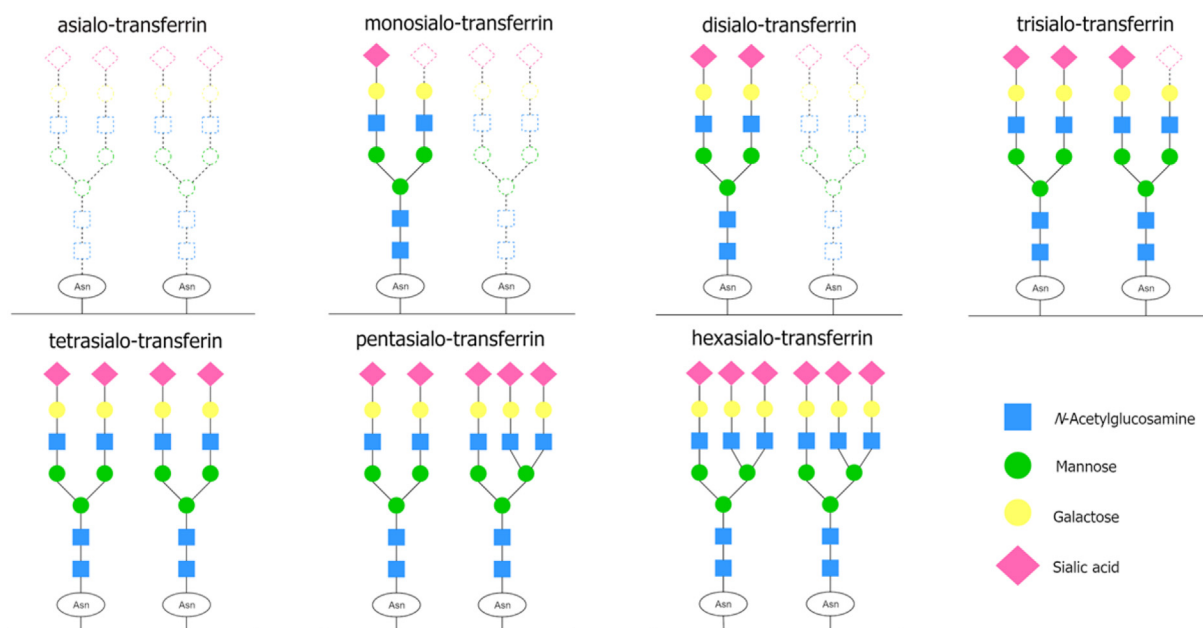

Figure 1. Schematic representation of the microheterogeneity of human transferrin glycoforms.

provide new implications for the function of transferrin sialylation patterns. Recently, it has been hypothesized that ferroptosis may be an important cause of multiple organ involvement in severe coronavirus disease 2019 (COVID-19) for a substantial proportion of patients who have lymphopenia, low serum iron levels, and multiple organ involvement [16]. Severe COVID-19 disease, caused by severe acute respiratory syndrome coronavirus 2 (SARS-CoV-2) has also been associated with disseminated intravascular coagulation and thrombosis, accompanied by an upregulated expression of transferrin in SARS-CoV-2-infected cells [17]. Notably, transferrin has been identified an important clotting regulator and an adjuster in the maintenance of blood coagulation balance [18]. Another recent report indicates that transferrin receptor is possible entry point for SARS-CoV-2 and a promising anti-COVID-19 target [19].

For further mechanistic studies, it is crucial to develop robust methods of preparation and characterization of transferrin sialoforms. The purpose of this study is to define the optimal transferrin desialylation procedure and then separate the desialylated apo-transferrin (Tf-S) from the native apo-transferrin (Tf+S) using low-pressure pH gradient ion exchange chromatography. Detailed *N*-glycan analysis and UV/Vis spectrophotometric characterization of the obtained Tf-S and Tf+S fractions is provided as a first step towards detailed iron binding and/or release studies.

2. Material and methods

2.1. Reagents

Native human apo-transferrin (Biorbyt, UK, cat. no. orb80927), sodium acetate trihydrate (Kemika, Croatia), calcium chloride (Lach-Ner, Croatia), sodium chloride (Kemika, Croatia), neuraminidase (Glyco-Cleave® Neuraminidase Kit, GALAB Technologies, Germany, cat. no. 132011), pISep Buffer Kit (CryoBioPhysica, USA, cat. no. 20055), hydrogen chloride (Carlo Erba Reagents, Italy, 37 % solution), sodium hydroxide (Kemika, Croatia, pellets 2–5 mm), sodium phosphate (Kemika, Croatia), guanidine hydrochloride (PanReac AppliChem, USA), MES (2-(*N*-morpholino)ethanesulfonic acid, Sigma Aldrich, USA) and potassium chloride (Alkaloid, North Macedonia) were used without further purification. Water used for experiments was double distilled in an all-glass apparatus. All experiments except the enzymatic desialylation were performed at room temperature.

2.2. Methods

2.2.1. Preparation of the desialylated protein

Desialylated apo-transferrin is prepared by incubation of immobilized neuraminidase enzyme beads suspension (Glycocleave) in the native apo-transferrin buffered stock solution (pH = 5.5, t = 38 °C). After the incubation period of 48 hours, the desialylated sample is collected, washed out and concentrated by centrifugal filtration. The complete protocol has been described elsewhere [20].

2.2.2. Separation and purification of desialylated protein

Sialoform separation is performed by using specialized pH gradient ion exchange chromatography buffers (pIsep). The mixture of fully desialylated apo-transferrin and native apo-transferrin is dissolved in the start buffer pIsep A (pH = 8) and injected onto HiTrap Q HP anion exchange chromatography columns (Cytiva, USA). Two 1 mL columns were serially connected for improved separation. Elution is done by single step linear gradient (0–100 % pIsep B, pH = 4) procedure using ÄKTA Start
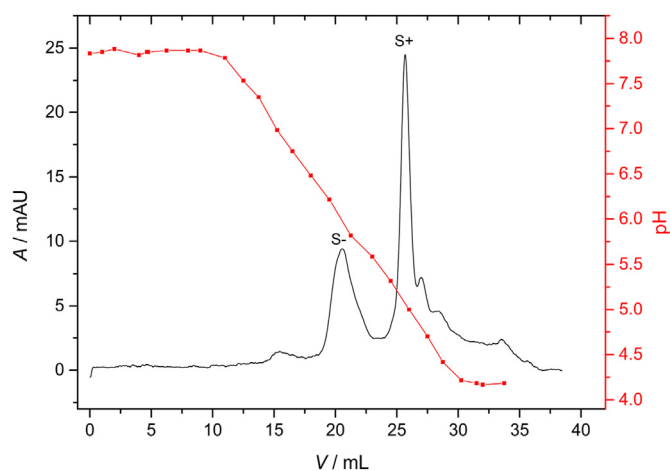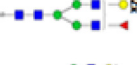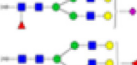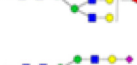

Figure 2. Low-pressure pH gradient ion exchange separation of native (S+) and desialylated (S-) human transferrin with two distinct signals matching different sialoforms, corresponding to 90 µg of Tf-S and 150 µg of Tf+S (black trace). The pH gradient obtained using pISep buffers is displayed as the red trace.

Table 1. Structure and content of *N*-glycans in the native and desialylated apo-transferrin, Tf+S and Tf-S, respectively, as determined by UPLC-MS. The *N*-glycan composition was determined by MS and the percent content of individual structures was calculated from the integrals of corresponding UPLC fluorescence signals [24]. The dominant fractions with a content $\geq$5% are printed in bold and make up approximately 90% of the total protein. The *IS* value corresponds to the proposed index of sialylation defined in Eq. (1).

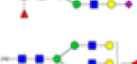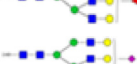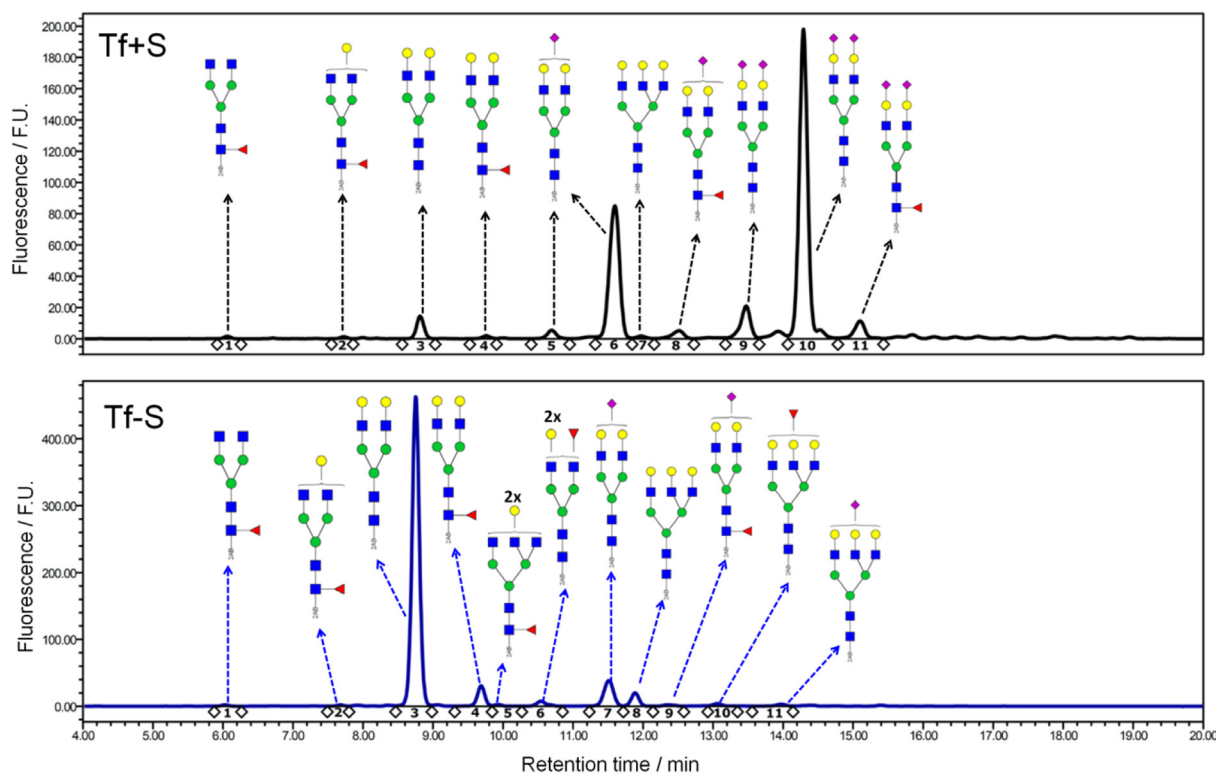| Native apo-transferrin (Tf+S): pI = 5.3; *IS* = 158.87				Desialylated apo-transferrin (Tf-S): pI = 6.5; *IS* = 9.76	
N-glycan composition*	Content / %	Schematic *N*-glycan structure**	*N*-glycan mass / [M+2H]²⁺ *Theoretical (Measured)*	*N*-glycan composition*	Content / %
1 FA2	0.36		792.314 (792.318)	1 FA2	0.35
2 FA2G1	0.31		873.340 (873.345)	2 FA2G1	0.35
3 A2G2	3.43		881.338 (881.343)	**3 A2G2**	**77.66**
4 FA2G2	0.52		954.367 (954.371)	**4 FA2G2**	**5.23**
			1055.906 (1055.910)	5 FA3G2	0.46
			954.367 (954.371)	6 A2F1G2	1.74
5 A2G2S1	**1.62**		1026.885 (1026.891)	**7 A2G2S1**	**8.39**
6 A2G2S1	**27.21**		1026.885 (1026.891)		
7 A3G3	0.54		1063.904 (1063.911)	8 A3G3	3.56
8 FA2G2S1	1.98		1099.914 (1099.920) 1136.933 (1136.939)	9 FA2G2S1 A3F1G3	0.56
9* A2G2S2**	**6.49**		1172.433 (1172.438)		
10* A2G2S2**	**53.70**		1172.433 (1172.441)		
11 FA2G2S2	3.84		1245.462 (1245.469)		
			1136.933 (1136.937)	10 A3F1G3	0.89
			1209.452 (1209.456)	11 A3G3S1	0.81

* Structure abbreviations: all *N*-glycans have two core *N*-acetylglucosamines (GlcNAc); Ax, number of antennae (GlcNAc) on trimannosyl core; A2, biantennary with both GlcNAcs as β1,2-linked; A3, triantennary with a GlcNAc linked β1,2 to both mannose and the third GlcNAc linked β1,4 to the α1,3 linked mannose; A4, GlcNAcs linked as A3 with additional GlcNAc β1,6 linked to α1,6 mannose; Gx, number (x) of β1,4 linked galactose on antenna; F(x), number (x) of fucose linked α1,3 to antenna GlcNAc; Sx, number (x) of sialic acids linked to galactose. [24,32]

** Schematic *N*-glycan structures: *N*-acetylglucosamine (■), mannose (●), galactose (●), fucose (▼), sialic acid (◆).

*** Structure A2G2S2 corresponds to a biantennary *N*-glycan with two terminal sialic acids that can be either α2,3 or α2,6 linked to galactose. These *N*-glycans have identical mass but can be separated by UPLC due to the different linkage and are therefore shown as separate fractions.

Figure 3. Structures of various *N*-glycan residues in the native apo-transferrin, Tf+S (black trace), and desialylated apo-transferrin, Tf-S (blue trace), as determined by UPLC-MS [24]. Schematic *N*-glycan structures and the corresponding fluorescence signals are indicated by arrows: *N*-acetylglucosamine (blue), mannose (green), galactose (yellow), fucose (red), sialic acid (pink).

Table 2. Structure and content of *N*-glycans in the desialylated apo-transferrin, Tf-S, for two separate batches run at different times from the same original batch of the native protein, as determined by UPLC-MS. The *N*-glycan composition was determined as described in Table 1. The *IS* value corresponds to the proposed index of sialylation defined in Eq. (1).

Desialylated apo-transferrin (Tf-S): pI = 6.5

Structure		Content/%		
		Fresh Enzyme	Recycled Enzyme*	Difference
1	FA2	0.35	0.46	-0.11
2	FA2G1	0.35	0.39	-0.04
3	A2G2	77.66	78.25	-0.59
4	FA2G2	5.23	5.95	-0.72
5	FA3G2	0.46	0.50	-0.04
6	A2F1G2	1.74	1.71	0.03
7	A2G2S1	8.39	7.80	0.59
8	A3G3	3.56	3.03	0.53
9	FA2G2S1 A3F1G3	0.56	0.61	-0.05
10	A3F1G3	0.89	0.53	0.36
11	A3G3S1	0.81	0.77	0.04
IS		9.76	9.18	-0.58

* Due to the decreased activity of the recycled enzyme, the incubation time was increased from 2 days (for the fresh enzyme) to 9 days (for the recycled enzyme).

protein purification system (Cytiva, USA). Protein concentration in the eluate is monitored by measuring absorbance at $\lambda = 280$ nm and protein fraction recovery can be calculated by integration over surface area (mL × mAU). After separation, the pH value of each fraction containing eluted protein was measured, corresponding to the approximate protein isoelectric point, pI. Full details of the pH-gradient chromatography have been described elsewhere [21].

2.2.3. Protein characterization by UPLC-MS

In order to verify the results of the enzymatic desialylation of the native protein and pH-gradient separation of different sialoforms, the complete *N*-glycan profiling of Tf+S and Tf-S was performed. Briefly, the protein *N*-glycans were released with the addition of 1.2 U of PNGase F (Promega, USA) and overnight incubation at 37° C. The released *N*-glycans were labeled with 2-aminobenzamide (Sigma Aldrich, USA) and purified using hydrophilic interaction liquid chromatography solid-phase extraction (HILIC-SPE). Fluorescently labeled *N*-glycans were separated by Acquity UPLC H-Class instrument (Waters, USA) using BEH Glycan chromatography column (Waters, USA). All glycan structures were annotated with MS/MS analysis using Synapt G2-Si ESI-QTOF-MS system (Waters, USA). Glycan compositions and structural features were assigned using software tools GlycoWorkbench and Glycomode, according to obtained MS and MS/MS spectra [22, 23]. Full details of the protein characterization by UPLC-MS have been described elsewhere [24].

2.2.4. Protein characterization by UV/Vis spectroscopy

In order to facilitate the determination of protein quantities in mechanistic studies, the molar absorption coefficients of both the native and desialylated protein were determined according to the modified Edelhoch method, as described elsewhere [25]. Briefly, the folded protein absorbance at 280 nm (A_{280}) was measured in 25 mM sodium phosphate buffer (pH = 7.4). The unfolded (denatured) protein absorbance at 280 nm ($A_{u\,280}$) was measured in the same buffer in the presence of 6 M guanidine HCl. The molar absorption coefficient of a folded protein at 280 nm (ε_{280}) is then equal to the product of a reference molar absorption coefficient for the unfolded protein, $\varepsilon_{u\,280}$, and the ratio of folded and unfolded protein absorbance, i.e. $\varepsilon_{280} = \varepsilon_{u\,280} \times A_{280}/A_{u\,280}$. The reference value of $\varepsilon_{u\,280} = 81080$ has been calculated from the contributions of 8 tryptophan, 26 tyrosine and 19 cystine residues in apo-transferrin structure [26, 27, 28]. The UV/Vis measurements were
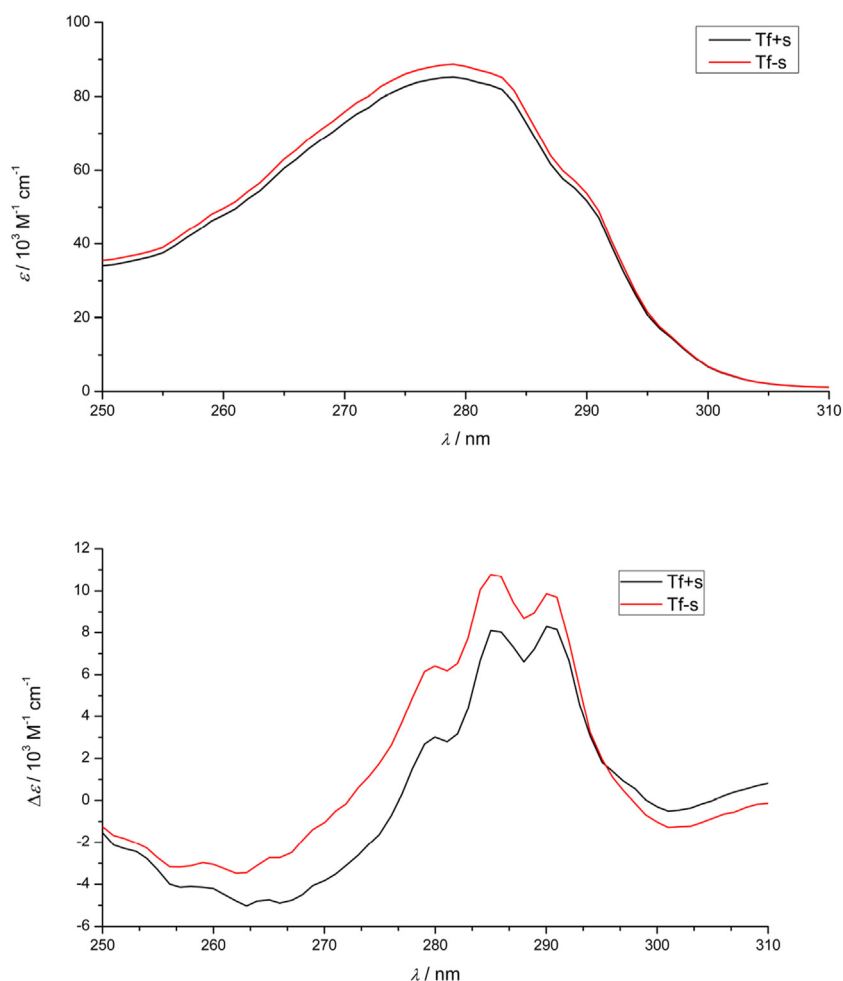
Figure 4. Top: The molar absorption coefficient, ε, of the Tf+S (black) and Tf-S (red) fractions in the near-UV range: ε_{280} (Tf+S) = $(84.8 \pm 0.2) \times 10^3$ M^{-1} cm^{-1} and ε_{280} (Tf-S) = $(88.2 \pm 0.2) \times 10^3$ M^{-1} cm^{-1}; Bottom: The difference in molar absorption coefficients, $\Delta\varepsilon$, for the intact and denatured proteins: Tf+S (black trace) and Tf-S (red trace). The values were calculated as $\Delta\varepsilon = \varepsilon_f - \varepsilon_u$, where ε_f is the molar absorption coefficient of the intact (folded) protein, and ε_u is the molar absorption coefficient of the denatured (folded) protein in 6 M guanidine [25].

performed on a Varian Cary 50 spectrophotometer (Varian, Australia) using a quartz cell with pathlength $l = 1$ cm (Hellma, Germany).

The dependence of native apo-transferrin absorbance (A_{280}) on salt concentration and pH was also measured in the range 0 M < [KCl] < 1.0 M and 4.9 < pH < 7.6. For salt concentration dependence, a stock solution of Tf+S was prepared in 25 mM sodium phosphate buffer (Buffer 1, pH = 7.4). Another buffer solution containing 25 mM sodium phosphate and 2 M KCl was also prepared (Buffer 2, pH = 7.4). To obtain samples with different total KCl concentrations, 100 μL of the stock transferrin solution was mixed with 100 μL of Buffer 1 and Buffer 2 mixtures in varying ratios to prepare working solutions with the final volume of 200 μL (final Tf+S concentration of 0.4 mg/mL). For measuring pH dependence, a stock solution of Tf+S was prepared in purified water. A buffer solution containing 50 mM MES, 50 mM sodium phosphate, and 0.4 M KCl (Buffer 3) was prepared separately and adjusted to pH values of 5.0, 5.5, 6.0, 6.5, 7.0, and 7.5 by adding an appropriate amount of 5 M NaOH. To obtain samples with different final pH, 100 μL of the stock transferrin solution was mixed with 100 μL of Buffer 3 to prepare working solutions with the final volume of 200 μL (final Tf+S concentration of 0.3 mg/mL). The final pH of the working solutions was measured using Mettler-Toledo MP 220 pH-meter (Mettler-Toledo, Switzerland) calibrated with standard buffer solutions (pH = 4.00 and pH = 7.00).

All samples were prepared in triplicate and A_{280} was measured for each sample in a quartz cell ($l = 1$ cm) using Varian Cary 50 spectrophotometer (Varian, Australia). The data were analyzed using a single factor ANOVA routine in Microsoft Excel Data Analysis Toolpak. If the calculated *P*-value is more than the chosen confidence level ($\alpha = 0.05$),

and the obtained *F*-value is less than the critical *F*-value, the null-hypothesis that there is no significant difference between the means of the samples should not be rejected [29].
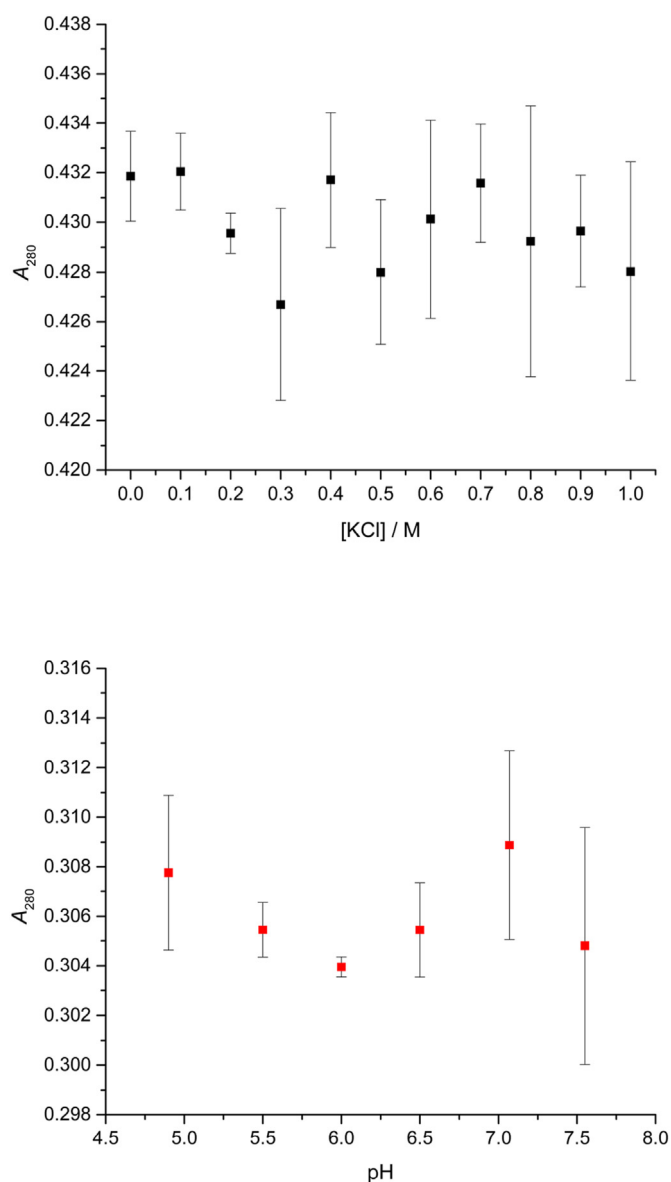
3. Results and discussion

3.1. Enzymatic desialylation

Compared to the original protocol [30], the concentration of working buffer was increased from 0.05 M to 0.2 M, thus increasing the desialylation capacity from 2 mg of protein to 5 mg of protein per reaction cycle, corresponding to 150 % increase in the reaction throughput. The final ratio is 1 mL of the immobilized enzyme suspension per 25 mg of protein. The desialylation enzyme is stable and can be used multiple times if an appropriate rinsing and preserving procedure is applied. However, the immobilized enzyme activity decreases after repeated use and increased incubation time is necessary to obtain comparable degree of protein desialylation. For successful desialylation, it is crucial to closely monitor the pH of the solution before and during the reaction (optimal pH = 5.5) and adjust accordingly by the addition of alkali. The reaction releases terminal sialic acids and unchecked acidification of the reaction mixture can inactivate the enzyme.

3.2. The pH chromatofocusing of native and desialylated transferrin

Initial attempts to form of externally controlled pH gradient in the range from pH = 8 to pH = 4 using either Servalyt (SERVA Electrophoresis, Germany) or Pharmalyte (Cytiva, USA) buffers were unsuccessful,

Table 3. Results of the single factor ANOVA routine in Microsoft Excel for the dependence of native transferrin (Tf+S) absorbance (A_{280}) on salt concentration. The average values and standard deviations of individual measurements are given in Figure 5, Top. The default confidence level for analysis is $\alpha = 0.05$.

Anova: Single Factor ($\alpha = 0.05$)					
Summary		A_{280}			
[KCl]/M	Count	Sum	Average	Standard deviation	Variance/10^6
0	3	1.2955	0.4318	0.0018	3.30
0.1	3	1.2961	0.4320	0.0016	2.42
0.2	3	1.2887	0.4296	0.0008	0.65
0.3	3	1.2801	0.4267	0.0039	14.9
0.4	3	1.2951	0.4317	0.0027	7.40
0.5	3	1.2840	0.4280	0.0029	8.51
0.6	3	1.2904	0.4301	0.0040	15.9
0.7	3	1.2947	0.4316	0.0024	5.67
0.8	3	1.2877	0.4292	0.0055	29.9
0.9	3	1.2889	0.4296	0.0023	5.06
1	3	1.2841	0.4280	0.0044	19.4

ANOVA*					
Source of Variation	SS/10^4	df	MS/10^5	F	P-value	F crit.
Between Groups	0.977	10	0.977	0.950	**0.510**	2.297
Within Groups	2.262	22	1.028			

* Definitions of parameters: *SS* represents the sum of squared deviations from the mean; *df* represents degrees of freedom; *MS* represents the mean square value; *F* represents the *F*-ratio; *F crit.* represents the critical *F*-value based on the *F*-distribution [29].

desialylated (pI $\approx$ 6) apo-transferrin differ significantly and hence can be fully separated (Figure 2).

3.3. The N-glycan analysis of the native and desialylated transferrin

In order to confirm the results of the pH chromatofocusing, both elution fractions, Tf+S and Tf-S, were analyzed by mass spectroscopy [24, 32]. The detailed *N*-glycan structure and quantification of transferrin sialoforms determined by UPLC-MS (Table 1 and Figure 3) shows that the native apo-transferrin (Tf+S) is dominated by glycan structures with 1 or 2 terminal sialic acid (A2G2S1 and A2G2S2) which together make up approximately 90 % of the total glycan content. Conversely, the *N*-glycan structures without the terminal sialic acids (A2G2, FA2G2) are dominant in desialylated apo-transferrin (Tf-S) and together make up approximately 90 % of the total glycan content. The applied protocol requires 100 μg of protein and should be repeated each time a new commercial sample is purchased and also after each desialylation cycle.

The reproducibility of the *N*-glycan content was tested for two separate batches run at different times from the same original batch of the native protein. The first batch of Tf-S was prepared with the fresh enzyme, whereas the second batch of Tf-S was prepared with the enzyme that has been recycled a number of times. Due to the decreased activity of the recycled enzyme, the incubation time was increased from 2 days (for the fresh enzyme) to 9 days (for the recycled enzyme). However, the content differences are within 1 % for every *N*-glycan fraction, as shown in Table 2.

According to the manufacturer's specifications, the used enzyme preferentially hydrolyzes α2,3 linkages of sialic acid, but will also cleave α2,6 and α2,8 linkages, with the preference for α2,3 linkages estimated at 260-fold [30]. This preference for α2,3 linked sialic acids might account for the observed incomplete desialylation of the native protein (approximately 10 % remaining sialylated *N*-glycan fractions).

For the purpose of simple comparison of the overall protein sialic acid content for different samples we propose a simple measure, *index of sialylation*, defined in Eq. (1):

Figure 5. Top: The dependence of Tf+S solution absorbance (A_{280}) on salt concentration: average values (black) and standard deviations (error bars) for triplicate samples, 0 M < [KCl] < 1.0 M, pH = 7.4; Bottom: The dependence of Tf+S solution absorbance (A_{280}) on pH: average values (red) and standard deviations (error bars) for triplicate samples, 4.9 < pH < 7.6, [KCl] = 0.2 M.

presumably due to insufficient buffering capacity at specific pH values (data not shown). However, a very linear pH gradient over the required pH range was achieved using pISep buffers that are specifically designed for chromatofocusing [31]. The pH gradient shown in Figure 2 (red trace) is linear in the range of 11–30 mL, corresponding to the range 7.78 > pH > 4.22 (R2 = 0.999). An additional improvement achieved using pISep buffer was in a significantly reduced absorbance baseline at 280 nm, making it easier to monitor protein elution from the column and more accurately calculate the amount of eluted protein by integrating chromatograms. However, the precise preparation of chromatofocusing buffers requires the special pISep pH gradient maker software.

Further improvement in transferrin sialoform separation was achieved by connecting two 1 mL HiTrap Q HP columns in a series, as compared to using only one 1 mL column. The two-column series backpressure of 0.15 MPa was well within the operational range of the ÄKTA Start system. The observed pI values for the native (pI $\approx$ 5) and

Table 4. Results of the single factor ANOVA routine in Microsoft Excel for the dependence of native transferrin (Tf+S) UV/Vis spectrum on pH. The average values and standard deviations of individual measurements are given in Figure 5, Bottom. The default confidence level for analysis is $\alpha = 0.05$.

Anova: Single Factor ($\alpha = 0.05$)

Summary		A_{280}			
pH	Count	Sum	Average	Standard deviation	Variance/10^6
4.9	3	0.9233	0.3078	0.0031	9.80
5.5	3	0.9163	0.3054	0.0011	1.22
6.0	3	0.9118	0.3039	0.0004	0.17
6.5	3	0.9163	0.3054	0.0019	3.66
7.1	3	0.9266	0.3089	0.0038	14.6
7.6	3	0.9144	0.3048	0.0048	22.9

ANOVA*

Source of Variation	SS/10^4	df	MS/10^5	F	P-value	F crit.
Between Groups	0.528	5	1.056	1.210	**0.362**	3.106
Within Groups	1.047	12	0.872			

* Definitions of parameters are the same as in Table 3.

$$IS = \sum_{i=1}^{n} f_i \times s_i, \tag{1}$$

where *IS* is the index of sialylation, *n* is the number of the *N*-glycan fraction, f_i is the % content of the particular *N*-glycan fraction and s_i is the number of sialic acids in the structure of the same *N*-glycan fraction. The composition of the native protein sample in Table 1 yields the value *IS* (Tf+S) = 158.87. For comparison, the desialylated protein sample in Table 1 yields the value *IS* (Tf-S) = 9.76, signifying 93.9 % reduction in the protein sialic acid content. Similar comparison of the desialylated protein samples in Table 2 yields only 0.58 % difference in the overall sialic acid content between Tf-S batches.

3.4. The molar absorption coefficients of the native and desialylated transferrin

The determined molar absorption coefficients in the near-UV range for of the Tf+S and Tf-S fractions, ε_{280} (Tf+S) = $(84.8 \pm 0.2) \times 10^3$ M^{-1} cm^{-1} and ε_{280} (Tf-S) = $(88.2 \pm 0.2) \times 10^3$ M^{-1} cm^{-1} (Figure 4, Top), will allow precise determination of concentrations in protein samples, which is important due to the variable water and salt content in commercial samples (up to 15 % w/w). The observed values of ε_{280} for the native and desialylated protein differ by approximately 4 %, probably due to the change in dielectric microenvironment. This effect can be attributed to interplay of the negatively charged sialic acid groups on the protein surface with aromatic amino acid residues in the protein structure. Alternatively, this effect can also arise from small conformational change in the protein due to different solvation of Tf+S and Tf-S caused by different surface charge. Such a small conformational change might indeed be the reason for the subtle variations in the Tf+S and Tf-S difference spectra obtained by denaturation in 6 M guanidine (Figure 4, Bottom) [25, 33, 34].

The measured absorbance of Tf+S at 280 nm shows no significant dependence on salt concentration up to 1 M KCl or pH in the range 4.9 < pH < 7.6 (Figure 5). The resulting *P*-value calculated using a single factor ANOVA routine in Microsoft Excel was greater than the default confidence level ($P > 0.05$), resulting in the acceptance of the null-hypothesis of equal means (Tables 3 and 4) [29].

These results will allow the precise determination of the molar absorption coefficients of iron-saturated transferrin species, as well as the determination of the fluorescence properties of the proteins. The applied protocol requires 1 mg of protein, of which 60 % can be reused for other measurements. Similarly to the *N*-glycan analysis, the molar absorption coefficients determination should also be repeated for each new native protein batch and each desialylation cycle due to possible variable sialic acid content.

4. Conclusions

Low-pressure pH gradient ion exchange separation provides a fast, simple and cost-effective method for preparative purification of native and desialylated apo-transferrin. The method enables easy monitoring of the extent of the desialylation reaction and also the efficient separation and purification of protein fractions after the desialylation reaction is terminated. Furthermore, the method can easily be modified for other glycoproteins and is particularly appropriate for quick testing of protein sialic acid content prior to verification by mass spectrometry. The *N*-glycan analysis shows that the modified desialylation protocol successfully reduces the content of the sialylated fractions relative to the native apo-transferrin. In the optimized protocol, the desialylation capacity is increased by 150 %, compared to the original protocol provided by the manufacturer.

In order to ensure the reproducibility of any further mechanistic studies, the complete *N*-glycan assignation and molar coefficients determination should be performed for each new native protein batch, as well as after every desialylation cycle. This is important because different native protein batches might have different *N*-glycan profiles, depending on the protein source. Additionally, the decreased enzyme activity after repeated use requires extended incubation time for sufficient desialylation. Importantly, the molar absorption coefficients of the native and desialylated apo-transferrin differ by several percent, suggesting that the literature data on glycoprotein molar absorption coefficients should be taken with caution because the measurement depends on the *N*-glycan composition of the protein, which is variable.

Acknowledgements

References

[1] K.W. Moremen, M. Tiemeyer, A.V. Nairn, Vertebrate protein glycosylation: diversity, synthesis and function, Nat. Rev. Mol. Cell Biol. 13 (2012) 448–462.

[2] A. Varki, R.D. Cummings, J.D. Esko, H.H. Freeze, P. Stanley, C.R. Bertozzi, G.W. Hart, M.E. Etzler (Eds.), Essentials of Glycobiology, second ed., Cold Spring Harbor Laboratory Press, Cold Spring Harbor (NY), 2009. http://www.ncbi.nlm.nih.gov/books/NBK1908/. (Accessed 12 February 2021).

[3] J. Alper, Searching for medicine's sweet spot, Science 291 (2001) 2338–2343.

[4] A. Kobata, A retrospective and prospective view of glycopathology, Glycoconj. J. 15 (1998) 323–331.

[5] H. Stibler, Carbohydrate-deficient transferrin in serum: a new marker of potentially harmful alcohol consumption reviewed, Clin. Chem. 37 (1991) 2029–2037.

[6] G. de Jong, H.G. van Eijk, Microheterogeneity of human serum transferrin: a biological phenomenon studied by isoelectric focusing in immobilized pH gradients, Electrophoresis 9 (1988) 589–598.

[7] S. Supraha Goreta, S. Dabelic, J. Dumic, Insights into complexity of congenital disorders of glycosylation, Biochem. Med. (2012) 156–170.

[8] P. König, H. Niederhofer, H. Steurer, R. Haller, R. Wölfle, H. Fritzsche, P. Weiss, Changes of carbohydrate-deficient transferrin in chronic, Alcoholism, Neuropsychobiology. 32 (1995) 192–196.

[9] T. Arndt, Carbohydrate-deficient transferrin as a marker of chronic alcohol abuse: a critical review of preanalysis, analysis, and interpretation, Clin. Chem. 47 (2001) 13–27.

[10] M. Grønbaek, J.H. Henriksen, U. Becker, Carbohydrate-deficient transferrin–a valid marker of alcoholism in population studies? Results from the Copenhagen City Heart Study, Alcohol Clin. Exp. Res. 19 (1995) 457–461.

[11] M. Edwards, F. McKenzie, S. O'callaghan, D. Somerset, P. Woodford, J. Spilsbury, M. Fietz, J. Fletcher, Prenatal diagnosis of congenital disorder of glycosylation type Ia (CDG-Ia) by cordocentesis and transferrin isoelectric focussing of serum of a 27-week fetus with non-immune hydrops, Prenat. Diagn. 26 (2006) 985–988.

[12] M. Piagnerelli, K.Z. Boudjeltia, V. Nuyens, D. De Backer, F. Su, Z. Wang, J.-L. Vincent, M. Vanhaeverbeek, Rapid alterations in transferrin sialylation during sepsis, Shock Augusta Ga 24 (2005) 48–52.

[13] Y. Beguin, G. Bergamaschi, H.A. Huebers, C.A. Finch, The behavior of asialotransferrin-iron in the rat, Am. J. Hematol. 29 (1988) 204–210.

[14] P. Lei, T. Bai, Y. Sun, Mechanisms of ferroptosis and relations with regulated cell death: a review, Front. Physiol. 10 (2019).

[15] T. Xu, W. Ding, X. Ji, X. Ao, Y. Liu, W. Yu, J. Wang, Molecular mechanisms of ferroptosis and its role in cancer therapy, J. Cell Mol. Med. 23 (2019) 4900–4912.

[16] M. Yang, C.L. Lai, SARS-CoV-2 infection: can ferroptosis be a potential treatment target for multiple organ involvement? Cell Death Dis. 6 (2020) 130.

[17] K.-M. McLaughlin, M. Bechtel, D. Bojkova, C. Münch, S. Ciesek, M.N. Wass, M. Michaelis, J. Cinatl, COVID-19-Related coagulopathy—is transferrin a missing link? Diagnostics 10 (2020) 539.

[18] X. Tang, Z. Zhang, M. Fang, Y. Han, G. Wang, S. Wang, M. Xue, Y. Li, L. Zhang, J. Wu, B. Yang, J. Mwangi, Q. Lu, X. Du, R. Lai, Transferrin plays a central role in coagulation balance by interacting with clotting factors, Cell Res. 30 (2020) 119–132.

[19] X. Tang, M. Yang, Z. Duan, Z. Liao, L. Liu, R. Cheng, M. Fang, G. Wang, H. Liu, J. Xu, P.M. Kamau, Z. Zhang, L. Yang, X. Zhao, X. Peng, R. Lai, Transferrin receptor is another receptor for SARS-CoV-2 entry, BioRxiv (2020).

[20] T. Friganović, V. Borko, T. Šeba, R. Kerep, I. Biruš, T. Weitner, Protocol for Enzymatic Desialylation of Native Apo-Transferrin, Zenodo, 2020.

[21] T. Friganović, V. Borko, T. Šeba, R. Kerep, T. Weitner, Protocol for pH-Gradient Chromatofocusing of the Native and Desialylated Human Apo-Transferrin, Zenodo, 2020.

[22] A. Ceroni, K. Maass, H. Geyer, R. Geyer, A. Dell, S.M. Haslam, GlycoWorkbench: a tool for the computer-assisted annotation of mass spectra of glycans, J. Proteome Res. 7 (2008) 1650–1659.

[23] C.A. Cooper, E. Gasteiger, N.H. Packer, GlycoMod–a software tool for determining glycosylation compositions from mass spectrometric data, Proteomics 1 (2001) 340–349.

[24] T. Štambuk, A. Cvetko, T. Weitner, Protocol for Ultra Performance Liquid Chromatography-Mass Spectrometry N-Glycan Analysis of the Native and Desialylated Human Apo-Transferrin, Zenodo, 2020.

[25] T. Šeba, T. Friganović, T. Weitner, Protocol for Spectrophotometric Determination of Native and Desialylated Apo-Transferrin Molar Absorption Coefficients, Zenodo, 2020.

[26] G.R. Grimsley, C.N. Pace, Spectrophotometric determination of protein concentration, Curr. Protein Pept. Sci. 33 (2003) 3.1.1–3.1.9.

[27] N.G. James, A.B. Mason, Protocol to determine accurate absorption coefficients for iron-containing transferrins, Anal. Biochem. 378 (2008) 202–207.

[28] S.C. Gill, P.H. von Hippel, Calculation of protein extinction coefficients from amino acid sequence data, Anal. Biochem. 182 (1989) 319–326.

[29] D.M. Bourg, Excel Scientific and Engineering Cookbook, first ed., O'Reilly, Sebastopol, CA, 2006.

[30] Product Description for GlycoCleave® Neuraminidase Kit, 2009.

[31] L.I. Tsonev, A.G. Hirsh, Theory and applications of a novel ion exchange chromatographic technology using controlled pH gradients for separating proteins on anionic and cationic stationary phases, J. Chromatogr. A 1200 (2008) 166–182.

[32] R. Saldova, A. Asadi Shehni, V.D. Haakensen, I. Steinfeld, M. Hilliard, I. Kifer, A. Helland, Z. Yakhini, A.-L. Børresen-Dale, P.M. Rudd, Association of N-glycosylation with breast carcinoma and systemic features using high-resolution quantitative UPLC, J. Proteome Res. 13 (2014) 2314–2327.

[33] A.P. Demchenko, Ultraviolet Spectroscopy of Proteins, Springer Berlin / Heidelberg, Berlin, Heidelberg, 2013.

[34] F.-X. Schmid, Biological macromolecules: UV-visible spectrophotometry, in: John Wiley & Sons, Ltd (Ed.), Encycl. Life Sci., John Wiley & Sons, Ltd, Chichester, UK, 2001.